



RESEARCH ARTICLE

10.1002/2014GC005469

Modeling ash fall distribution from a Yellowstone supereruption

Larry G. Mastin¹, Alexa R. Van Eaton², and Jacob B. Lowenstern³

¹U.S. Geological Survey, Cascades Volcano Observatory, Vancouver, Washington, USA, ²School of Earth and Space Exploration, Arizona State University, Tempe, Arizona, USA, ³U.S. Geological Survey, Yellowstone Volcano Observatory, Menlo Park, California, USA

Key Points:

- We model tephra fall from a Yellowstone supereruption
- Growth of an umbrella cloud was considered
- Umbrella cloud may drive ash >1500km upwind

Supporting Information:

- Readme
- Simulation results
- Wind data

Correspondence to:

L. G. Mastin,
lgmastin@usgs.gov

Citation:

Mastin, L. G., A. R. Van Eaton, and J. B. Lowenstern (2014), Modeling ash fall distribution from a Yellowstone supereruption, *Geochem. Geophys. Geosyst.*, 15, 3459–3475, doi:10.1002/2014GC005469.

Received 26 JUN 2014

Accepted 28 JUL 2014

Published online 27 AUG 2014

This is an open access article under the terms of the Creative Commons Attribution-NonCommercial-NoDerivs License, which permits use and distribution in any medium, provided the original work is properly cited, the use is non-commercial and no modifications or adaptations are made.

Abstract We used the volcanic ash transport and dispersion model Ash3d to estimate the distribution of ashfall that would result from a modern-day Plinian supereruption at Yellowstone volcano. The simulations required modifying Ash3d to consider growth of a continent-scale umbrella cloud and its interaction with ambient wind fields. We simulated eruptions lasting 3 days, 1 week, and 1 month, each producing 330 km³ of volcanic ash, dense-rock equivalent (DRE). Results demonstrate that radial expansion of the umbrella cloud is capable of driving ash upwind (westward) and crosswind (N-S) in excess of 1500 km, producing more-or-less radially symmetric isopachs that are only secondarily modified by ambient wind. Deposit thicknesses are decimeters to meters in the northern Rocky Mountains, centimeters to decimeters in the northern Midwest, and millimeters to centimeters on the East, West, and Gulf Coasts. Umbrella cloud growth may explain the extremely widespread dispersal of the ~640 ka and 2.1 Ma Yellowstone tephra deposits in the eastern Pacific, northeastern California, southern California, and South Texas.

1. Introduction

The consequences of a future, caldera-forming eruption from Yellowstone have been the subject of much speculation but little quantitative research in terms of regional ashfall impacts. Despite graphic and often fanciful media depictions of the devastation and the impact on human life that would result from a modern supereruption (producing >1000 km³ volcanic ash or >400 km³ DRE of magma), no historical examples exist from which to draw comparison [Self, 2006]. The largest eruptions of the past few centuries have produced a few to several tens of cubic kilometers of magma. Examples include Tambora volcano, Indonesia in 1815 [Oppenheimer, 2003], Krakatau in 1883 [Simkin and Fiske, 1983], the Katmai/Valley of Ten Thousand Smokes eruption, Alaska in 1912 [Hildreth, 1983], Quizapu volcano, Chile in 1932 [Hildreth and Drake, 1992], and most recently, Pinatubo, Philippines in 1991 [Newhall and Punongbayan, 1996]. These erupted volumes are much larger than the Mount St. Helens eruption in 1980 (0.2–0.4 km³) [Pallister et al., 1992], but at least an order of magnitude smaller than the largest Yellowstone events [Christiansen and Blank, 1972].

From geological evidence, we know that ash from the last large eruptions at Yellowstone (2.1 Ma, 1.3 Ma, and 640 ka) spread over many tens of thousands of square kilometers. These tephra deposits however have been remobilized in the millennia after emplacement, and estimates of primary ash thickness are challenging to obtain. Widespread Yellowstone-derived deposits, known as the “Pearlette ash beds,” have been important stratigraphic markers throughout the central and western United States and Canada (Figure 1), even before their volcanic source location was recognized [Wilcox and Naeser, 1992]. Izett and Wilcox [1982] listed nearly 300 locations for Yellowstone ashes spread as widely as California, Texas, Iowa and Saskatchewan. Over 3 m of ash from the Lava Creek Tuff eruption (640 ka) are found in north-central Texas. In the Gulf of Mexico, tens of meters of ash-dominated deposits were emplaced immediately following the 2.1 Ma Huckleberry Ridge Tuff eruption [Dobson et al., 1991] and the later Lava Creek eruption. The great thickness of these and other deposits [Izett and Wilcox, 1982] partially reflects fluvial and (or) aeolian reworking, obscuring the primary distribution of ash thicknesses. In this study, we address the following questions: (1) given modern meteorological patterns, where and how much ash would be deposited by a Yellowstone supereruption? (2) how sensitive is the thickness distribution to changes in the season and duration of eruptive pulses? and (3) what is the long-term (probabilistic) estimate of ashfall distribution?

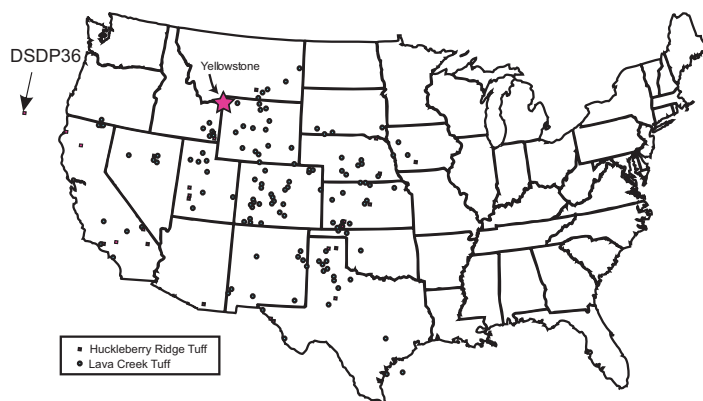


Figure 1. Location of sites where distal ashes from the Huckleberry Ridge Tuff (2.1 Ma) and Lava Creek Tuff (640 ka) eruptions have been identified [Izett and Wilcox, 1982], with some additional sites from A. Sarna-Wojcicki, personal communication, March 2013). “DSDP 36” refers to Deep-Sea Drill Hole 36, whose core contains Yellowstone ash deposits as described by Sarna-Wojcicki et al. [1987].

2. Methodology

We investigate these questions using the volcanic ash transport and dispersion model Ash3d [Schwaiger et al., 2012]. Ash3d is a finite-volume Eulerian model that calculates tephra transport by dividing the atmosphere into a three-dimensional grid of cells, placing tephra particles into cells above the volcano, and calculating their flux through cell walls as tephra is advected by wind and falls at a settling velocity determined by its size, density, and shape.

Ash3d also calculates turbulent diffusion using a Crank-Nicolson formulation with either a constant or variable diffusivity. Diffusivity has been adjusted in modeling studies to match the observed rate of downwind widening of a deposit or ash cloud, with different values required to match different observations [Bonadonna et al., 2005; Folch et al., 2009]. This procedure likely replicates the effects of more than one process, such as turbulent entrainment in weak plumes [Bonadonna et al., 2005], or umbrella cloud spreading in strong plumes [Costa et al., 2013]. Its effect is to increase the dispersal of ash; a process already accounted for to an exceptional degree by umbrella cloud spreading. Thus for simplicity we set diffusion to zero in these simulations.

The standard version of Ash3d places tephra into a column of source nodes above the volcano and distributes it vertically using a simple formula [Suzuki, 1983] designed to concentrate mass near the plume top:

$$\frac{d\dot{M}}{dz} = \dot{M} \frac{k_s^2 (1 - z/H_T) \exp(k_s(z/H_T - 1))}{H_T [1 - (1 + k_s) \exp(-k_s)]} \quad (1)$$

Here \dot{M} is the mass flow rate into the plume, H_T is the height of the plume top, z is the elevation at a particular point in the column, and k_s is an adjustable constant that controls the degree to which mass is concentrated near the top of the column. Example curves using $k_s=4, 8,$ and 12 are shown in Figures 2a–2c (right side).

Approximating the plume as a column of source nodes is adequate for weak plumes (Figure 2a), and those with moderate-sized umbrella clouds (Figure 2b), so long as they do not extend much farther upwind than a typical cell width. A supereruption however could drive an umbrella cloud thousands of kilometers upwind [Baines and Sparks, 2005]. Clouds of this scale are fed by a column which rises buoyantly to a maximum height (H_T , Figure 2c), then collapses downward and outward as a density current that spreads radially at its neutral density elevation (H_u , Figure 2c). Their volume rate of growth dV/dt is proportional to the volume rate \dot{V} at which the rising column feeds the cloud [Sparks et al., 1986; Sparks et al., 1997, section 11.2]:

$$\frac{dV}{dt} = \dot{V} \quad (2)$$

From dimensional considerations, \dot{V} has been inferred to follow the relationship [Morton et al., 1956; Sparks, 1986],

$$\dot{V} \approx C \sqrt{k_e} \frac{\dot{M}^{3/4}}{N^{5/8}}, \quad (3)$$

where k_e is the radial entrainment coefficient of the rising plume and N is the Brunt-Väisälä frequency. C is a constant of proportionality, empirically determined through 3-D modeling to be $\sim 0.5 \times 10^4 \text{ m}^3 \text{ kg}^{-3/4} \text{ s}^{-7/8}$ in tropical eruptions and $1 \times 10^4 \text{ m}^3 \text{ kg}^{-3/4} \text{ s}^{-7/8}$ in midlatitude and polar eruptions [Suzuki and Koyaguchi, 2009]. We use $k_e=0.1, C=1 \times 10^4 \text{ m}^3 \text{ kg}^{-3/4} \text{ s}^{-7/8}$, and $N=0.02 \text{ s}^{-1}$ in our calculations.

The pressure gradient dP/dr driving outward motion results largely from the head drop between the cloud top (H_T , Figure 2c) and the neutral buoyancy elevation (H_u) [Sparks et al., 1997, equation (11.5)],

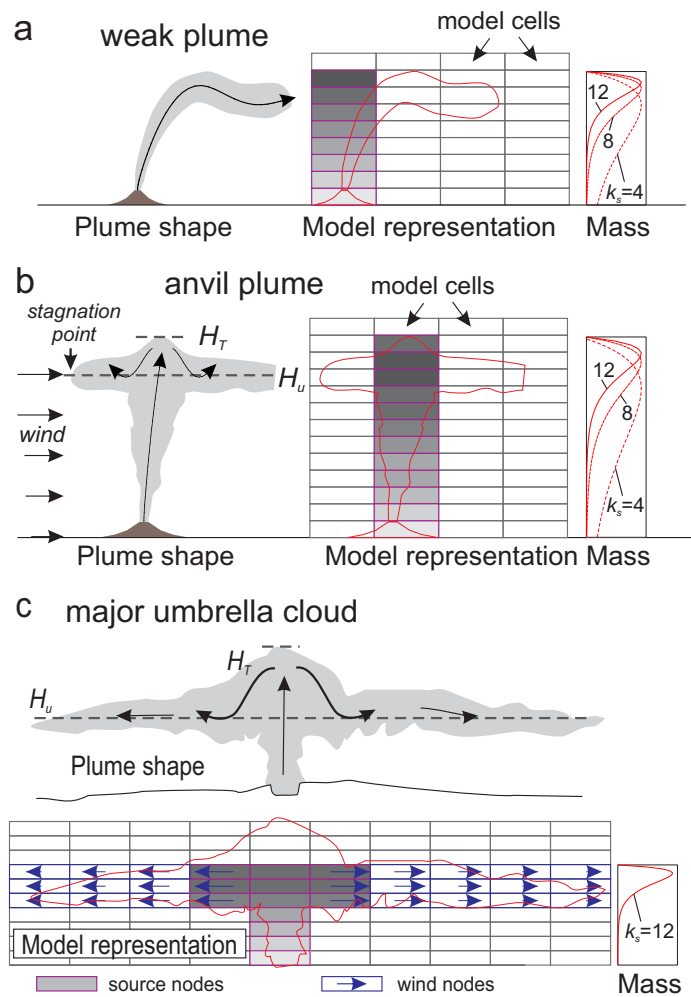


Figure 2. Illustrations and model representations of (a) a weak plumes; (b) a strong plume that develops an anvil cloud (i.e., an umbrella cloud that is truncated on the upwind side); and (c) a major umbrella cloud. On the right-hand side of each subfigure are curves showing the distribution of mass with elevation, calculated using equation (1), with values of k_s as labeled. Gray nodes with magenta outlines are source nodes, to which ash is added at each time step in the model. Nodes with blue outlines are wind nodes, in which a radial wind field is added to simulate umbrella cloud expansion.

The expansion speed of the cloud's outer margin, u_R , can be estimated by taking the derivative of equation (5) with time [Costa et al., 2013]:

$$u_R = \frac{2}{3} \left(\frac{3\lambda N\dot{V}}{2\pi} \right)^{1/3} t^{-1/3}. \quad (6)$$

Within the cloud, ash is assumed to spread at a radial velocity u_r , that approaches u_R as $r \rightarrow R$. Assuming a cylindrical cloud geometry and a nondivergent flow field, this leads to the relation [Costa et al., 2013]:

$$u_r = \frac{3}{4} u_R \frac{R}{r} \left(1 + \frac{1}{3} \frac{r^2}{R^2} \right). \quad (7)$$

We implemented these relationships in Ash3d using a modification of the method of Costa et al. [2013]. Specifically, an arrangement of source nodes consisting of a 3×3 matrix of cells (in plan view) extends over the upper 25% of the plume height, from the base to the top of the umbrella cloud (we do not include an overshooting top in our simulations) (Figures 2c, 3b, and 3c). From the vent elevation to the base of the

$$\frac{dP}{dr} = (\rho_c - \rho_a)g \frac{H_T - H_U}{R}, \quad (4)$$

where R is cloud radius, ρ_c is the mean cloud density, ρ_a is ambient air density at the neutral buoyancy elevation, and g is gravitational acceleration.

Equations (2) and (4) account for conservation of mass and momentum in the cloud, respectively. They have been combined and integrated, with certain substitutions given in Sparks et al. [1997, chap. 11] to derive the following formula for cloud radius with time t [Costa et al., 2013, equation (1); Sparks et al., 1997, equation (11.8); Suzuki and Koyaguchi, 2009, equation (2)],

$$R = \left(\frac{3\lambda N\dot{V}}{2\pi} \right)^{1/3} t^{2/3}, \quad (5)$$

where λ is a factor reflecting cloud shape, whose value has been estimated at ~ 0.2 from 3-D modeling [Suzuki and Koyaguchi, 2009]. This equation has been shown to match the rate of growth observed in the 1991 Pinatubo eruption cloud [Holasek et al., 1996; Sparks et al., 1997, Figure 11.3] and in 3-D numerical simulations [Suzuki and Koyaguchi, 2009].

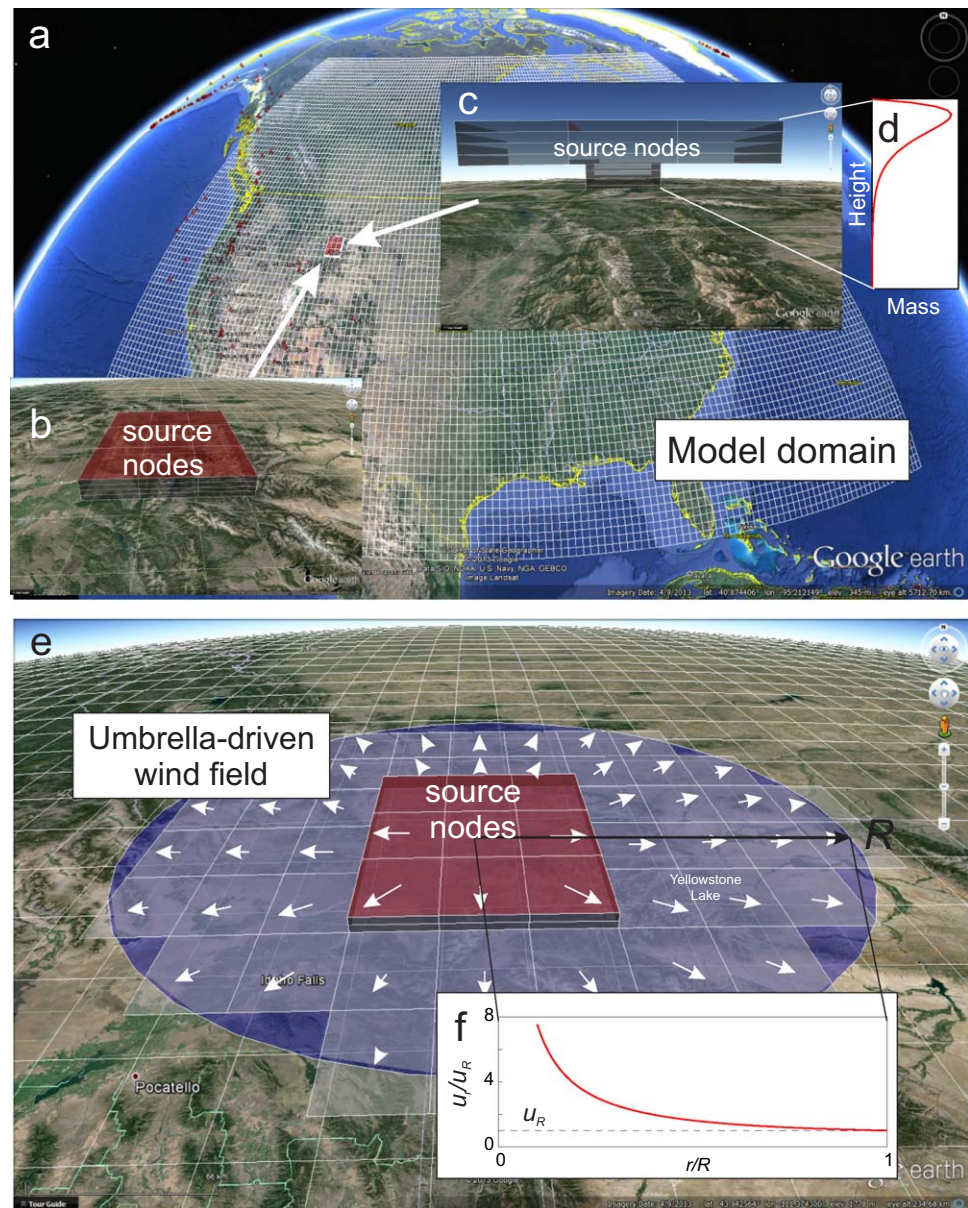


Figure 3. (a) Illustration in Google Earth® of the model domain used for the Yellowstone model simulations. Our simulations used a grid spacing 0.5 degrees latitude and longitude, and 4 km cell height. (b) Top and (c) side view (looking north) of the source nodes above Yellowstone from which ash is dispersed. (d) Distribution of mass with height in the source nodes. (e) Radial wind field (white arrows) added to the ambient wind field in the umbrella region (purple). (f) Radial wind speed u_r/u_R in the cloud. Copyrighted images by Google (2011), Europa Technologies (2011), Tele Atlas, and Geocenter Consulting. Use of these images is consistent with usage allowed by Google (<http://www.google.com/permissions/geoguidelines.html>) and do not require explicit permission for publication.

umbrella cloud, the eruption plume source consists of a single column of nodes as in the standard version of Ash3d. At the beginning of each simulation, we calculate \dot{V} from equation (3). Then, at each time step, the existing tephra in each 3×3 layer of source nodes is averaged; new tephra is added to these cells according to the mass eruption rate, and distributed vertically using equation (1) with a top-heavy k_s of 12 (Figures 2c and 3d). Within each layer of cells, tephra mass is evenly distributed horizontally. Then, the cloud radius at that time step is calculated using equation (5) and, within the umbrella (purple region, Figure 3e), a radial wind field is calculated using equation (7) and added to the ambient wind field.

This method differs slightly from that of *Costa et al.* [2013] in that it uses equation (5) to calculate umbrella-cloud radius at any given time rather than an equation that integrates dR/dt . This modification requires that

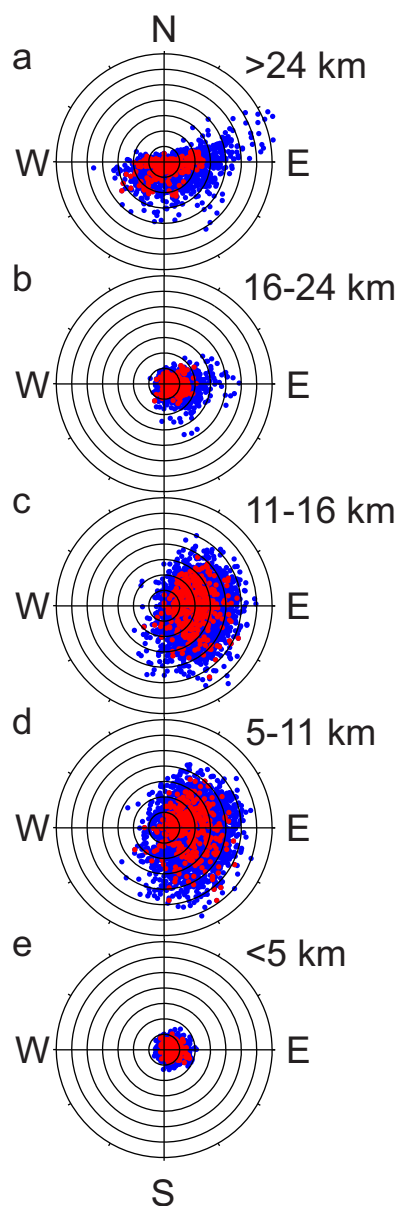


Figure 4. Plots of wind direction and speed at Yellowstone at elevations of >24 km (a), 16–24 km (b), 11–16 km (c), 5–11 km (d), and <5 km (e). The radial position of each dot represents the wind speed, from zero (center) to 70 m s^{-1} (outermost circle); the azimuthal location represents the direction toward which the wind is blowing, with true north in the up direction. Blue dots represent all daily data from 1 January 2000 to 31 December 2010, whereas the red dots represent data for 2001.

3.2. Volcanic Inputs

For erupted volume, we chose a fixed value of 330 km^3 dense-rock equivalent (DRE) of magma. The three major caldera-forming eruptions from Yellowstone that produced the Huckleberry Ridge Tuff, Mesa Falls Tuff, and Lava Creek Tuff expelled about 2450, 280, and 1000 km^3 DRE of magma, respectively [Christiansen, 2001]. But only a fraction of this volume rose in buoyant ash columns that could be carried by winds to form fall deposits; the remainder was emplaced either as ignimbrites that spread along the ground or as intracaldera fill that remained within the structural depression formed by collapse. The amount of these eruptions emplaced as tephra fall deposits is not well known, but is likely tens of percent based on

the eruption be specified as a single pulse of constant plume height and eruption rate rather than a time series of heights and rates.

The appendix A provides a validation of this approach by comparing Ash3d simulations to the well-documented growth of the 1991 Pinatubo umbrella cloud. Ash3d does not resolve the dynamics of eruption plume ascent – instead, the height and vertical distribution of mass are held constant throughout the eruption. Despite a highly parameterized depiction of the plume, the model's key strength is its ability to examine the long-distance umbrella expansion and dispersal of erupted material in a complex, time-varying wind field.

3. Model inputs

Inputs to the model include a 3-D time-varying meteorological wind field; volume of magma erupted; eruption start time; eruption duration; column height; and the size, density, and shape factor of erupted fragments. Our choice of inputs is described below.

3.1. Meteorological Inputs

For meteorology, we use historical wind patterns represented in the NOAA NCEP/NCAR Reanalysis 1 model [Kalnay *et al.*, 1996] (RE1). Model output gives the wind field every 6 h on a 3-D grid spaced at 2.5° intervals in latitude and longitude, and at 17 pressure levels in the atmosphere, from 1000 mb (sea level) to 10 mb (about 34 km elevation). Wind vectors in the RE1 grid are linearly interpolated in space and time onto our grid at every time step. We have chosen representative time periods from the year 2001 for our simulations. This year was not strongly influenced by swings in either the El Niño Southern Oscillation (ENSO) [Di Lorenzo *et al.*, 2010] or the Pacific Decadal Oscillation (PDO) [Mantua and Hare, 2002]. Wind speeds and directions above Yellowstone for this year (Figure 4, red dots) show reasonable agreement with longer-term patterns between 2000 and 2010 (blue dots).

Table 1. Grain-Size Distribution GSD1, Used in Most Model Simulations

Size (mm)	Mass Fraction	Density (kg/m ³)
2	0.25	800
1	0.15	800
0.5	0.20	1000
0.25	0.15	1000
0.125	0.20	1800
0.0625	0.05	2000

better-studied, recent caldera-forming eruptions [e.g., Bacon, 1983; Wilson, 2001, 2008]. For our model simulations, the 330 km³ volume represents about one to two thirds of the total volume of a 500–1000 km³ eruption, which is above the threshold for a supereruption (1000 km³ bulk or ~400 km³ DRE) [Sparks et al., 2005]. Expulsion of 330 km³ DRE of magma in a week would imply a mass eruption rate of 7 × 10⁸ kg s⁻¹, assuming a magma density of 2500 kg m⁻³. This is comparable to the

~3–10 × 10⁸ kg s⁻¹ estimated for Pinatubo [Holasek et al., 1996; Koyaguchi and Ohno, 2001; Suzuki and Koyaguchi, 2009].

For eruption duration, we explore values from days to a month, reflecting durations that have been inferred and observed for moderate to large eruptions. The 1912 Novarupta eruption in Alaska, the largest volcanic eruption of the 20th century, ejected 15 km³ of magma over about 52 h [Hildreth, 1983]. The Tambora eruption of 1815, the largest in recent centuries, ejected about 50 km³ in 24 h [Self et al., 1984]. The climactic phase of the 1883 Krakatau eruption ejected 10 km³ of magma in about 36 h [Simkin and Fiske, 1983]. Field evidence from deposits of the 0.76 Ma Bishop Tuff from the Long Valley Caldera in California suggest that ~700 km³ magma was emplaced in a matter of days [Wilson and Hildreth, 1997]. On the other hand, Wilson [2008] estimates that the ~26 ka Oruanui eruption was a series of large-scale outbreaks of increasing vigor, including multiple hiatuses of up to several weeks. Many smaller eruptions have persisted for weeks or even months. Eyjafjallajökull volcano in Iceland, whose eruption shut down air space over Europe in April and May of 2010, erupted about 0.2 km³ magma in 59 days [Gudmundsson et al., 2012].

For the height of ash injection, several factors are considered. Plume height is known to correlate with eruption rate, suggesting that a high-flux Yellowstone eruption would produce a very high plume. But such correlations [e.g., Mastin et al., 2009, equation (1); Sparks et al., 1997, equation (5.1)] are based mainly on plumes that emanate from single, central vents, whereas a large, complex Yellowstone plume is more likely to rise from multiple vents, or as an elutriated ash cloud from pyroclastic flows. The 15 June, 1991 eruption of Pinatubo produce the highest historically observed plume of ~40 km [Holasek et al., 1996], but its umbrella cloud spread at much lower heights of about 18–25 km [Fero et al., 2009; Holasek et al., 1996; Suzuki and Koyaguchi, 2009]. Based on these observations, most of our simulations use an umbrella cloud whose top is at 25 km. We also explore end-member values of 15 km and 35 km.

For a particle-size distribution, we run most simulations using values listed in Table 1, referred to as GSD1. The size distribution primarily determines how the deposit is distributed with distance from the vent, with

Table 2. Grain-Size Distributions GSD2 and GSD3

	Size (mm)	GSD2 Moderate Aggregation Mass Fraction	GSD3 Weak Aggregation Mass Fraction	Density (kg/m ³)
Individual particles	1	0.043	0.043	1955
	0.707	0.021	0.021	2209
	0.5	0.046	0.046	2612
	0.354	0.072	0.072	2634
	0.25	0.053	0.053	2624
	0.177	0.029	0.029	2690
	0.125	0	0.033	2664
	0.088	0	0.046	2697
	0.063	0	0.060	2698
	0.044	0	0.070	2640
	0.031	0	0.060	2581
	0.022	0	0.021	2570
	Aggregate classes for GSD2	0.297	0.184	0
0.250		0.184	0	600
0.210		0.184	0	600
0.177		0.184	0	600
Aggregate class for GSD3	0.200	0	0.445	200

coarse particles settling near the vent and fine particles settling at greater distance. Ash3d calculates the settling rate of individual particles of ellipsoidal shape using relations of Wilson and Huang [1979], and a shape factor F ($F = (b+c)/2a$, where a , b , and c are the semimajor, intermediate, and semiminor axes of the ellipsoid, that is the average of tephra particles measured by Wilson and Huang [1979]. In real eruptions, particles smaller than about 0.063 to 0.125 mm aggregate into clusters and fall out faster than they would as

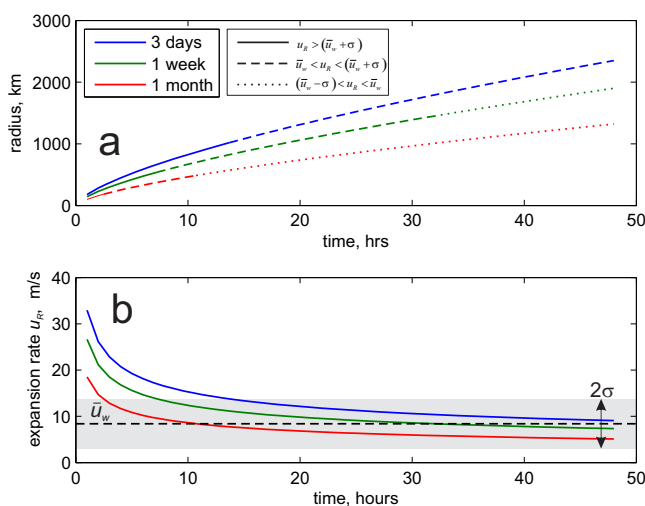


Figure 5. (a) Radius of the umbrella cloud versus time for eruption rates that correspond with eruption durations of 3 days (blue), 1 week (green), and 1 month (red). Symbols, and dashed and dotted segments are explained in the text. (b) Expansion rate u_R of these clouds versus time. The dashed black line represents the mean wind speed at 16–24 km elevation above Yellowstone, obtained by averaging RE 1 data for the years 2000–2010. The shaded gray zone encompasses one standard deviation on each side of this mean.

aggregation (A.R. Van Eaton et al., unpublished manuscript, 2014). Although a modern Yellowstone eruption may interact with external water (e.g., the 350 km² Yellowstone Lake) magma-water ratios would likely be higher than in the 2009 Redoubt eruption. Therefore, we consider two size distributions that represent less aggregation. The moderately aggregated GSD2 (Table 2) uses a modification of the total grain-size distribution (TGSD) of the 18 May 1980 Mount St. Helens deposit estimated by *Durant et al.* [2009, supporting information file 2008jb005756-txts03.txt], which integrated the deposit to a downwind distance of 671 km. To simplify calculations, we consolidated all tephra coarser than 1 mm into a single 1 mm size class. We then simulate aggregation by moving ash ≤ 0.125 mm diameter into four aggregate classes of size 0.177, 0.210, 0.250, and 0.297 mm with density 600 kg m⁻³, comparable to ash aggregates of low to intermediate density [*Van Eaton et al.*, 2012]. This scheme can reproduce the 18 May 1980 Mount St. Helens tephra fall distribution in Ash3d simulations [*Mastin et al.*, 2013a], and is reasonably consistent with field observations by *Sorem* [1982] that much of the very fine ash fell as clusters 0.25–0.5 mm diameter in the distal area. The weakly aggregated GSD3 (Table 2) starts with the Mount St. Helens TGSD of *Durant et al.* [2009], consolidates the coarser particles as above, and then moves 25% of the 0.031 mm particles, 75% of the 0.022 mm particles, and all particles smaller than 0.022 mm into a single aggregate class of 0.20 mm size and a density of 200 kg m⁻³. *Cornell et al.* [1983] used this scheme to reproduce 38 ka Campanian Y-5 tephra at Campi Flegrei, Italy, a deposit of >60–100 km³ volume DRE [*Cramp et al.*, 1989].

4. Results

4.1. Calculated Growth of the Umbrella Cloud

Tephra distribution from a large-scale explosive eruption would be influenced both by growth of the umbrella cloud and by the ambient wind field. Umbrella clouds propagate upwind until the spreading velocity equals the ambient wind velocity, at which point the leading edge stagnates (Figure 2b) [*Carey and Sparks*, 1986]. Locations upwind of the stagnation point are unlikely to receive tephra fall deposits. Figure 5a plots the cloud radius with time using equation (5) for an eruption lasting 3 days (blue lines), 1 week (green), and 1 month (red). The expansion rate u_R at the cloud's leading edge, calculated from equation (6) is shown in Figure 5b and compared with the mean wind speed \bar{u}_w (black dashed line) at 16–24 km elevation above Yellowstone, obtained from RE1 data for 2000–2010 (Figure 4). The shaded gray region covers the range of wind speeds one standard deviation (σ) above and below the mean for this time period. Solid, dashed, and dotted line segments in Figure 5a indicate segments of the growth curve in which $u_R > (\bar{u}_w + \sigma)$, $\bar{u}_w < u_R < (\bar{u}_w + \sigma)$, and $(\bar{u}_w - \sigma) < u_R < \bar{u}_w$, respectively.

individual particles [*Van Eaton et al.*, 2012]. The physics governing the rate of aggregation is an area of active research and not yet explicitly resolved by Ash3d.

To account for these effects, however, we consider a range of grain size distributions (GSD) that have been adjusted to match observed deposits. GSD1 has been adjusted to reproduce a heavily aggregated deposit—the 23 March 2009 (event 5) eruption of Redoubt Volcano, Alaska [*Mastin et al.*, 2013b]. This eruption was small (~ 1.6 M m³ DRE) [*Wallace et al.*, 2013] and mixed with abundant external water from a crater-filling glacier, resulting in extensive ash

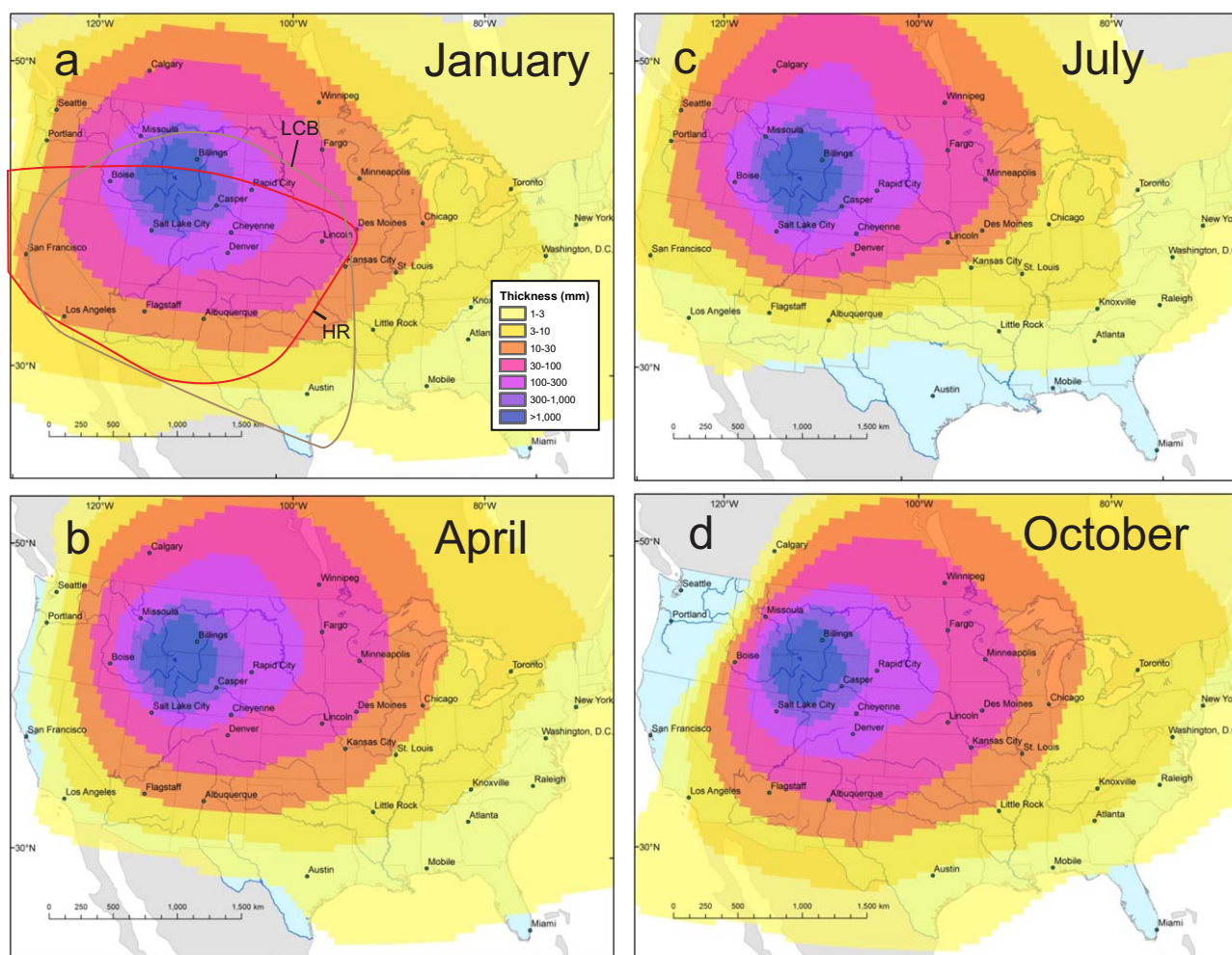


Figure 6. Simulated tephra fall thickness resulting from a month-long Yellowstone eruption of 330 km^3 using 2001 wind fields for (a) January, (b) April, (c) July, and (d) October. In (a), the bold red line delineates the extent of the Huckleberry Ridge Tuff Bed (HR); the brown line delineates the extent of Lava Creek B Tuff (LCB) [Sarna-Wojcicki, 2000].

These results show that, for the 3-day eruption, the expansion rate at the leading edge of the cloud could exceed the mean ambient wind speed for a period of days, producing a cloud that extends $>2000 \text{ km}$ upwind. For eruptions lasting a month or more, the expansion rate exceeds the mean wind speed for only several hours, producing a cloud whose maximum upwind extent is perhaps hundreds of kilometers.

4.2. Simulation Results

Figures 6–8 illustrate the simulated tephra thickness distribution in the conterminous United States and southern Canada for eruptions of 330 km^3 DRE lasting a month (Figure 6), a week (Figure 7), and 3 days (Figure 8). Parts a, b, c, and d, in each figure illustrate seasonal effects, showing results in wind fields calculated for winter (a), spring (b), summer (c), and fall (d). For comparison, Figure 9 illustrates month-long (a), week-long (b), and 3-day (c) eruptions in winter using simulations that do not account for the presence of an umbrella cloud.

One feature is clear in Figures 6–8: proximal isopachs depicting $>10 \text{ mm}$ tephra thickness are mostly circular to elliptical and don't vary dramatically in size, shape, or coverage with season or with eruption duration. The shape of thinner isopachs (1 and 3mm tephra) vary more strongly in response to variations in the ambient wind field.

Comparison of simulations with an umbrella cloud (Figures 6–8) and without (Figure 9) reveal two important differences. First, neglecting the physics of umbrella propagation, patterns of tephra deposition are more sensitive to the spatiotemporal variations in the wind field. For example, the briefest eruption (3 days; Figure 9c) produces a relatively narrow tephra deposit that extends toward the southwest. Second,

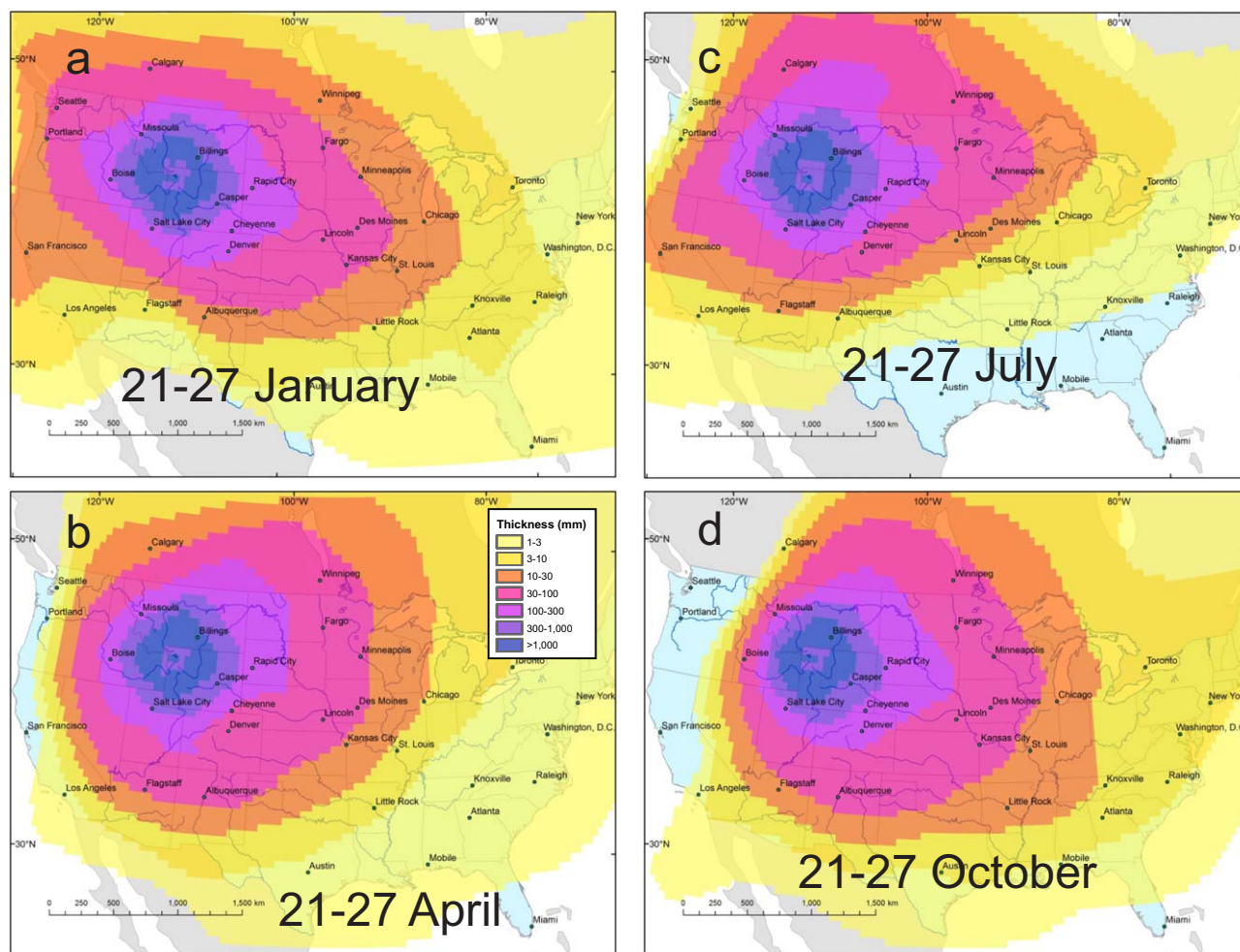


Figure 7. Simulated tephra fall thickness resulting from a week-long Yellowstone eruption of 330 km^3 using 2001 wind fields for (a) 21–27 January, (b) 21–27 April, 21–27 July, and (d) 21–27 October.

simulations with an umbrella cloud produce ash deposits that are much more widely dispersed. Without the umbrella cloud for example, the 10 mm isopach in the 3-day example (Figure 9c) covers 1.2 million km^2 ; with the umbrella cloud (Figure 6a), it covers 5.4 million—4.5 times the area.

Table 3 lists the average, maximum, and minimum tephra-fall thicknesses for cities shown in Figures 6–8. Cities within 500 km such as Billings and Casper are covered by tens of centimeters to more than a meter of ash, upper Midwestern cities such as Minneapolis and Des Moines receive centimeters, and those in the East and Gulf Coasts receive millimeters or less. California cities receive millimeters to centimeters. And Pacific Northwest cities of Portland and Seattle receive up to a few centimeters.

The concentric pattern of isopachs suggests the possibility that tephra thicknesses might be expressed as a simple function of distance from the volcano. Figure 10 illustrates tephra-fall thickness as a function of distance from Yellowstone for cities listed in Table 3. A general decrease in thickness with distance is apparent, although cities west of Yellowstone (indicated by black arrows and labels) receive much less ash overall than cities farther east. There is no clear difference in thickness distributions between month-long, week-long, and 3-day eruptions.

4.2.1. Effects of Column Height and Grain-Size Distribution

Modern observations have supported the fundamental concept that eruption column height has a strong influence on tephra distribution [Carey and Sparks, 1986]. However, Figures 11a and 11b, which illustrate depositional patterns from an umbrella cloud at 15 and 35 km height, respectively, don't differ greatly from

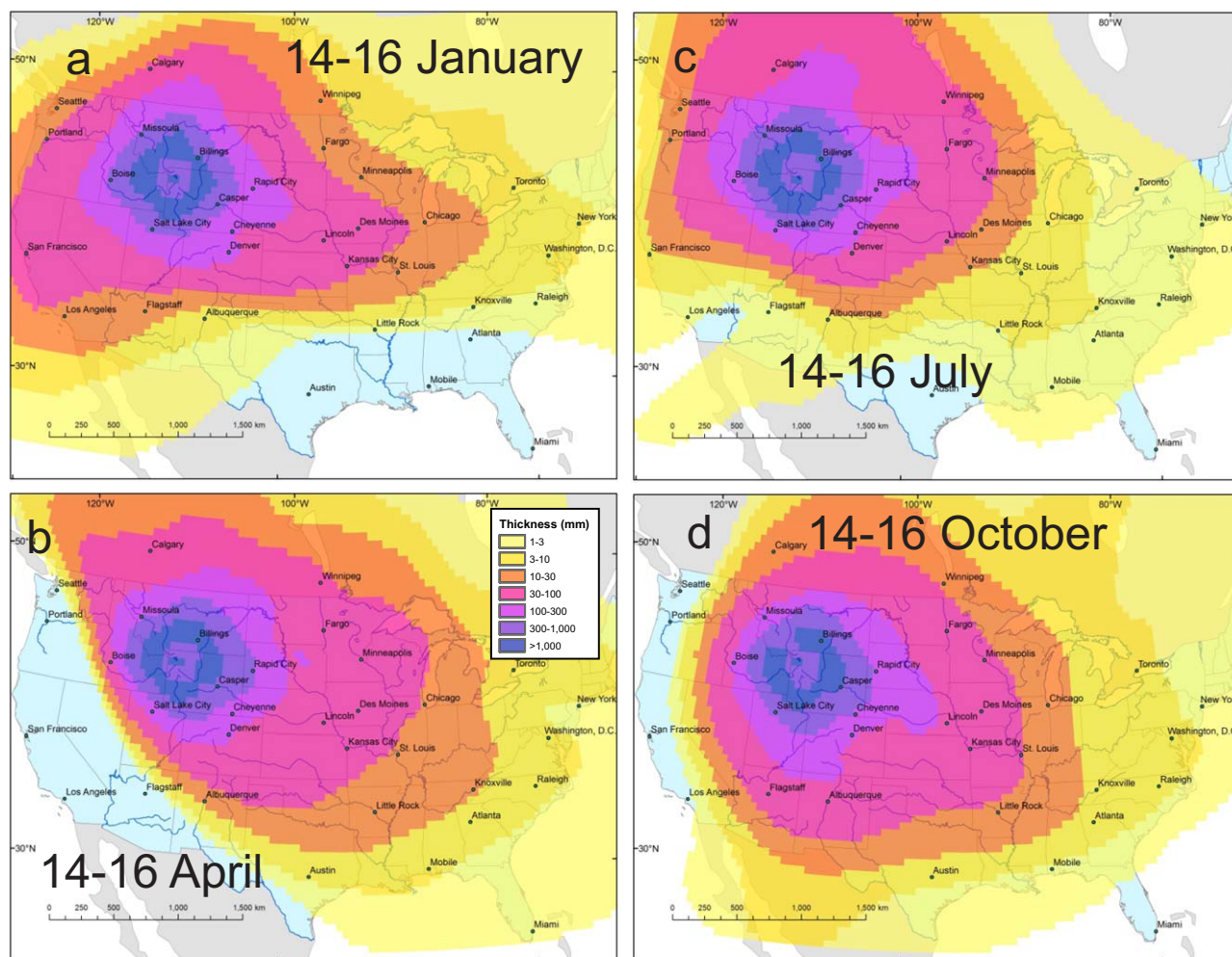


Figure 8. Simulated tephra fall thickness resulting from a 3-day-long Yellowstone eruption of 330 km^3 using 2001 wind fields for (a) 14–16 January, (b) 14–16 April, (c) 14–16 July, and (d) 14–16 October.

the 25 km column height (Figure 7b). The implication is that the dynamics of the powerfully spreading umbrella cloud dominates tephra dispersal in very large eruptions.

Grain-size distribution, however, does significantly affect tephra dispersal. This is illustrated in Figures 11c and 11d using grain-size distributions GSD2 and GSD3 for the 21–27 April simulation. The moderately aggregated GSD2 grain-size distribution, which is derived from the Mount St. Helens 18 May 1980 distal ash, shows similar dispersal to the heavily aggregated GSD1 (Figure 7b). In contrast, the weakly aggregated GSD3 shows much more widespread dispersal. Model results using GSD3 show that East Coast cities such as Washington, D.C., receive more than a centimeter, as opposed to the millimeters forecast under most GSD1 scenarios. The greater dispersal of the GSD3 size distribution likely results from the small size (0.2 mm) and low density (200 kg m^{-3}) of the single aggregate class, which contains 44% of the erupted mass. The true range of aggregate sizes and densities that might develop during such an eruption is difficult to anticipate, would depend strongly on atmospheric conditions, and is clearly an important factor to consider in long-distance ash dispersal.

The weakly aggregated GSD3 also places much more ash into distal clouds. The 21–27 April simulations using GSD1 and GSD2 deposited 97.5% and 99.7% of their erupted mass within the model domain. But the GSD3 simulation in Figure 11d sent 23.8% of the erupted mass beyond the model-domain boundary as an airborne cloud.

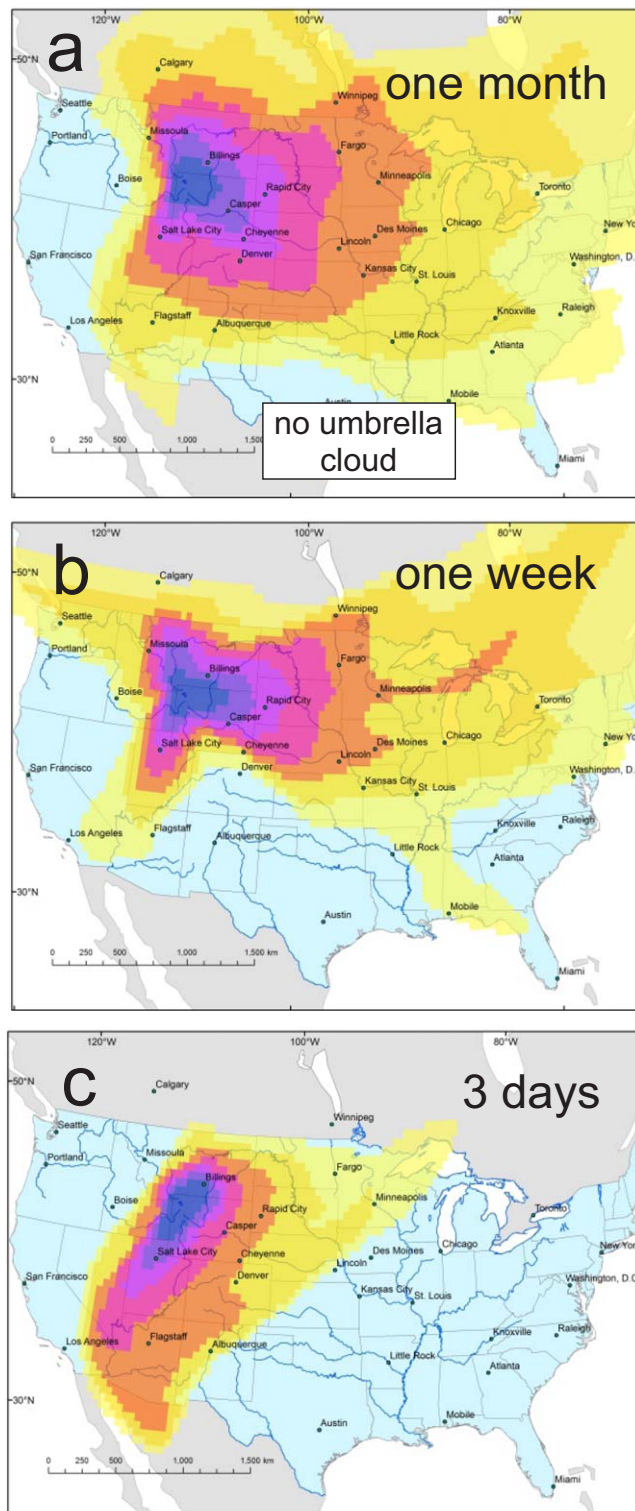


Figure 9. Results of simulations with no umbrella cloud: (a) 1 month (January); 1 week (21–27 January); and 3 days (14–16 January). Total plume height for these eruptions is 30 km. Deposit thickness is represented by the same colors as shown in Figures 6–8.

slope of the line. In equations (9) and (10), T_1 and T_2 are the intercepts, and k_1 and k_2 are the negative slopes, of the proximal and distal lines respectively. The term $A_{ip}^{1/2}$ represents the x coordinate at which the two lines intersect. Figure 12a plots a single best-fit line through each data set as dashed lines, and a

5. Discussion

The simulations described above disperse tephra over distances that are qualitatively consistent with dispersal characteristics of known supereruption deposits. In most of our simulations, tephra thicknesses >1 cm cover a few to several million square kilometers. For comparison, the ~ 170 km³ (DRE), ~ 26 ka Oruanui fall deposit, the most recent and best preserved of any supereruption, covered more than a million km² with ash thicknesses >1 cm [Wilson, 2001, Figure 9b]. The ~ 800 km³ (DRE), 74 ka Toba fall deposit covered more than about 7 million km² with >10 cm [Rose and Chesner, 1987].

To examine how ash dispersal from the Yellowstone simulations compares with other deposits, Figure 12a shows results on a plot of log thickness T versus square root area, $A^{1/2}$ [Pyle, 1989] for the 21–27 April simulations using grain-size distributions GSD1, GSD2, and GSD3. Using this method, the rate of thinning is expressed as either a single best-fit line [e.g., Fierstein and Nathenson, 1992; Pyle, 1989], according to:

$$T = T_0 \exp(-kA^{1/2}), \quad (8)$$

or as two line segments, using the following equations:

$$T = T_1 \exp(-k_1 A^{1/2}), \quad (9)$$

$$A^{1/2} < A_{ip}^{1/2},$$

$$T = T_2 \exp(-k_2 A^{1/2}), \quad (10)$$

$$A^{1/2} > A_{ip}^{1/2}.$$

In equation (8), T_0 is the y intercept and k is the negative

Table 3. Average, Maximum, and Minimum Deposit Thicknesses at Selected Cities, From Simulations Illustrated in Figures 6–8^a

City	Distance km	Longitude	Latitude	Thickness (mm)		
				Average	Minimum	Maximum
Albuquerque	1091	-106.61	35.111	24.9	4.1	73.9
Atlanta	2556	-84.387	33.748	3.1	0.5	6.5
Austin	1942	-97.743	30.267	2	0.1	4.2
Billings	227	-108.501	45.783	1429.5	1028.7	1785.6
Boise	452	-116.215	43.619	144.8	26.9	347.9
Calgary	777	-114.058	51.045	32.8	1.8	68.2
Casper	391	-106.313	42.867	516.9	325.9	844.3
Cheyenne	600	-104.82	41.14	152.9	96.3	274.4
Chicago	1887	-87.63	41.877	14.9	5.5	29.4
Denver	700	-104.985	39.737	98.1	63.6	131.9
Des Moines	1420	-93.609	41.601	40	19.3	59.6
Fargo	1111	-96.789	46.877	57.7	22.9	78.6
Flagstaff	1028	-111.639	35.201	16.3	0	50.6
Kansas City	1454	-94.621	39.114	31.7	7	57.2
Knoxville	2455	-83.92	35.96	4.3	1.2	10.5
Lincoln	1211	-96.682	40.807	52.9	22.6	88.5
Little Rock	1905	-92.289	34.746	8.4	1.6	25.2
Los Angeles	1323	-118.244	34.052	5.2	0	27
Miami	3453	-80.226	25.788	0.5	0	1.7
Minneapolis	1374	-93.267	44.983	39.2	23.2	53.5
Missoula	375	-114.019	46.86	240.6	48	474.4
Mobile	2508	-88.043	30.694	1.8	0.1	3.9
New York	3025	-74.004	40.714	2.5	1.4	3.7
Portland	950	-122.676	45.523	8.3	0	30.6
Raleigh	2884	-78.639	35.772	2.7	0.8	4.5
Rapid City	593	-103.231	44.08	208.3	168.2	330.2
St. Louis	1819	-90.199	38.627	15.3	3	32.5
Salt Lake City	419	-111.891	40.761	247.9	124.9	408.3
San Francisco	1229	-122.419	37.775	8.5	0	44.7
Seattle	966	-122.332	47.606	9.2	0	41.2
Toronto	2498	-79.383	43.653	3.7	2	6.2
Washington DC	2855	-77.036	38.907	2.9	1.3	4.4
Winnipeg	1188	-97.137	49.899	37.9	14.3	59.1

^a"Distance" is the distance in km from Yellowstone. Longitude is given in degrees east, latitude in degrees north.

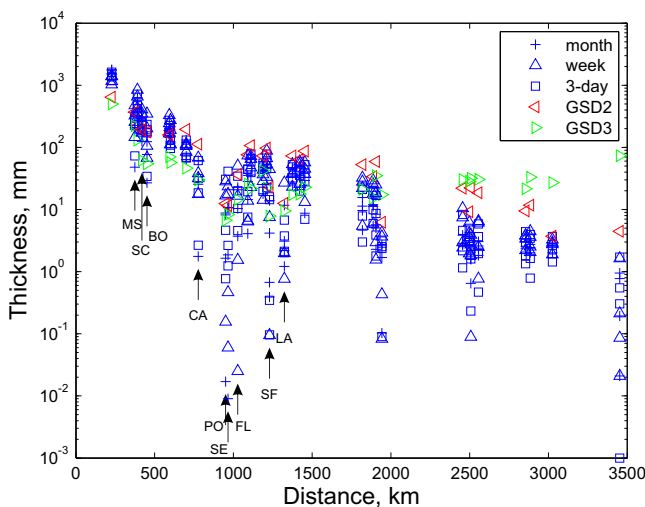


Figure 10. Tephra deposit thickness (mm) versus distance, for cities listed in Table 3 and shown in Figures 6–8. All blue symbols are for simulations illustrated in Figures 6–8, with crosses, triangles, and squares representing month-long, week-long, and 3-day eruptions respectively. Red and green symbols represent eruptions using grain-size distribution GSD2 and GSD3, illustrated in Figures 11c and 11d, respectively. Cities with longitudes west of Yellowstone are indicated by black arrows and labels: MS=Missoula, SC=Salt Lake City; BO=Boise; CA=Casper; PO=Portland; SE=Seattle; FL=Flagstaff; SF=San Francisco; LA=Los Angeles.

two-line best fit as dotted lines, using an automatic procedure for picking the slopes and intercepts of these two lines that minimizes the squared residuals.

Fierstein and Nathenson [1992] compiled values from the literature and found the slowest deposit thinning rates (lowest slopes) were associated with the largest, most widely dispersed eruptions. Figure 12b illustrates this trend by plotting the log of k and k_2 versus the log of bulk (not DRE) tephra volume, using data from Fierstein and Nathenson [1992, Table 6] along with one data point representing the distal slope of the Oruanui deposit [Wilson, 2001]. Regardless of whether one

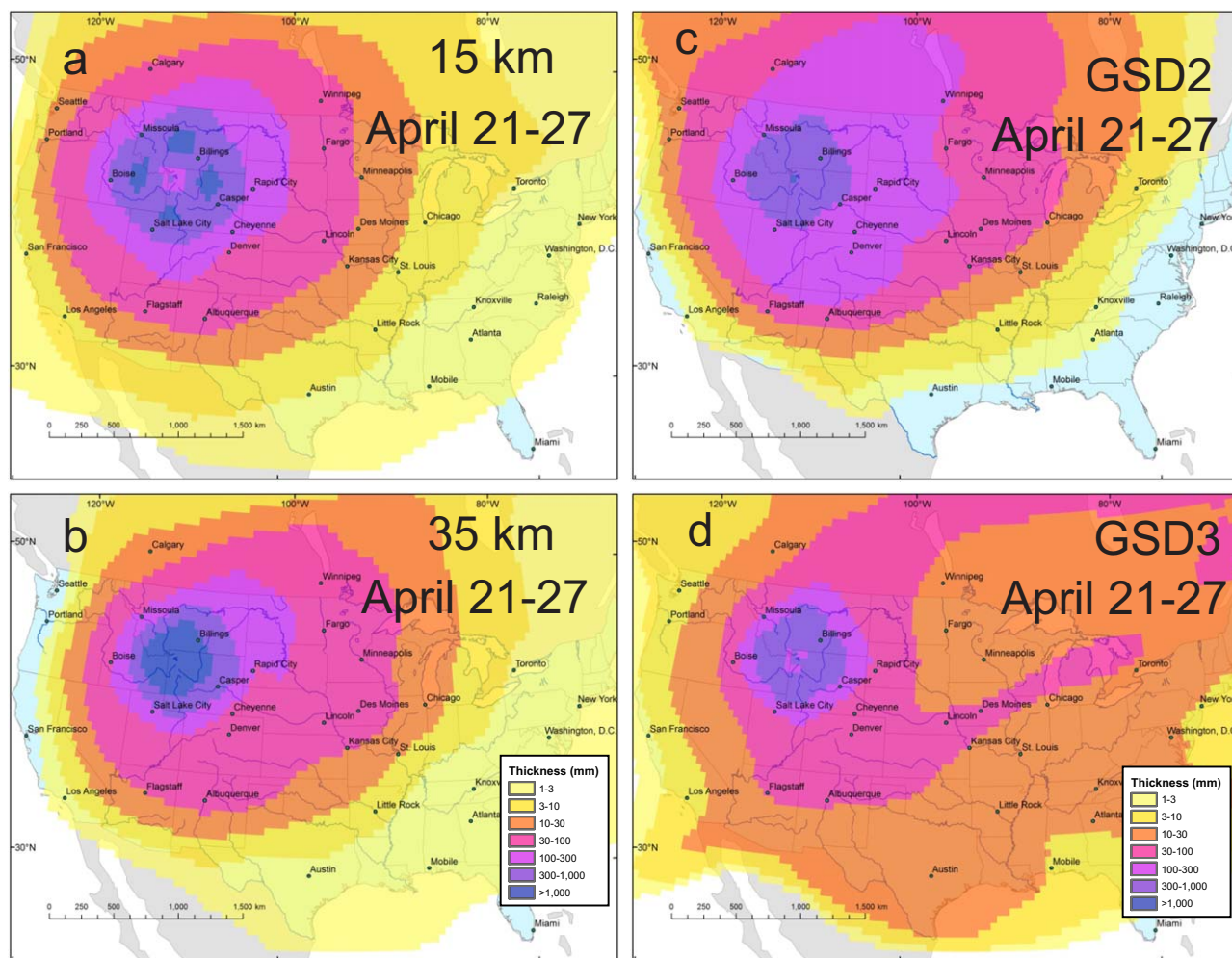


Figure 11. Tephra fall thickness for simulations from 21 to 27 April, using (a) a 15 km umbrella-cloud height, (b) a 35 km umbrella-cloud height, (c) grain-size distribution GSD2, and (d) grain-size distribution GSD3.

considers the total data set or separates out points for k or k_2 , a downward trend with increasing volume is visible at volumes $> \sim 1 \text{ km}^3$. At the right side of the plot, lying along the trend line, are values of k and k_2 from the three Yellowstone simulations in Figure 12a. Their location along this trend line suggests that the simulated tephra dispersal is reasonable for an eruption of this size.

These results portray a dramatically different picture of the ashfall hazard from a caldera-forming supereruption than one might expect based on traditional tephra transport models, which tend to neglect the physics of an expanding umbrella cloud. The distribution of tephra from such a large eruption is less sensitive to the wind field than that of smaller eruptions. It is also more widespread, and radially symmetric about the vent. The wide dispersal of tephra in our simulations results from rapid expansion of the umbrella rather than from a high plume or variability in the wind field at the umbrella spreading level during prolonged activity.

5.1. Immediate Ash Thickness Versus Long-Term Impact

North America's highest population density lies along its coastlines. Deposit thicknesses on the coasts from nearly all simulations is millimeters to a few centimeters. Thicknesses of this magnitude seem small but their effects are far from negligible. A few millimeters of ash can reduce traction on roads and runways [Guffanti et al., 2009], short out electrical transformers [Wilson et al., 2012] and cause respiratory problems [Horwell and Baxter, 2006]. Ash fall thicknesses of centimeters throughout the American Midwest would disrupt livestock and crop production, especially during critical times in the growing season. Thick deposits could

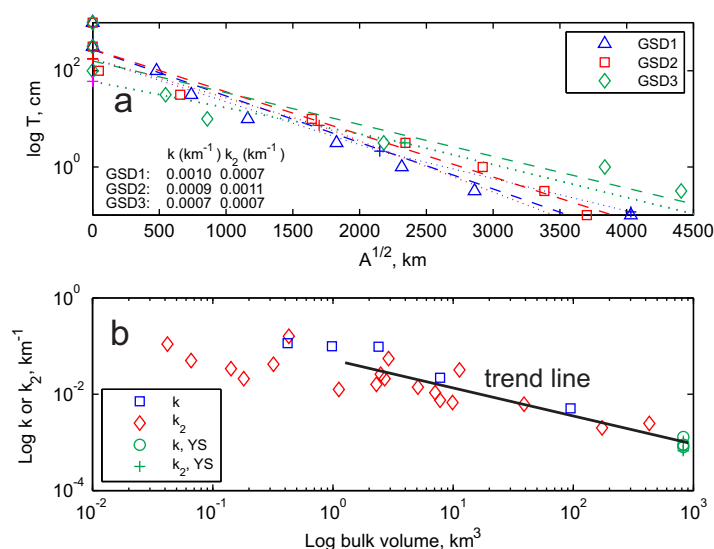


Figure 12. (a) Log of deposit thickness (cm) versus square root of area covered (km) for simulations using grain-size distributions GSD1 (blue triangles), GSD2 (red squares), and GSD3 (green diamonds) from 21 to 27 April. Dashed lines indicate best-fit lines through these data, fit using equation (5). Dotted lines indicate a two-line best fit in which the slopes and intercepts are automatically chosen to minimize squared residuals. The intersection of the two lines is indicated by a cross. Also listed are the best-fit values of k and k_2 . (b) Plot of k or k_2 versus log bulk erupted volume for tephra deposits compiled in Fierstein and Nathenson [1992, Table 6], plus the value of k_2 estimated by Wilson [2001] for the ~26 ka Oruanui tephra fall. Also shown are values of k and k_2 for the Yellowstone deposits illustrated in Figure 12a (green circles and crosses). Note that the x axis in Figure 12b represents bulk volume, consistent with values listed by Fierstein and Nathenson [1992] rather than DRE volume used elsewhere in this paper.

threaten building integrity and obstruct sewer and water lines [Wilson et al., 2012]. Electronic communications and air transportation would likely be shut down throughout North America. There would also be major climate effects. Emission of sulfur aerosols during the 1991 Pinatubo eruption produced global cooling by an average of 1° C for a few years, while the 50 km³ Tambora eruption of 1815 cooled the planet enough to produce the famed “year without a summer” in 1816, during which snow fell in June in eastern North America and crop failures led to the worst famine of the 19th century [Oppenheimer, 2003]. Other indirect effects include wind reworking of tephra into migrating dunes that bury roads and structures; or increased sediment load to streams that exacerbates flooding and impedes river traffic.

5.2. Comparison With Reported Locations of Yellowstone Ash Deposits

These simulations help us understand the extremely widespread distribution of the Huckleberry Ridge and Lava Creek eruption deposits from Yellowstone. Even under modern-day prevailing winds (blowing dominantly to the east), the influence of a large umbrella cloud results in millimeters to centimeters of ash accumulation in southern California (Figures 6–8), which is consistent with field observations (Figure 1). Likewise, the presence of thick deposits of Huckleberry Ridge and Lava Creek Tuffs in Pleistocene Lake Tecopa in southeastern California [Zett and Wilcox, 1982] requires significant ashfall at least as far as southern Nevada to feed the ancestral Amargosa River. In the Los Angeles Basin, both eruptions delivered significant ash to the river systems in that area; whether windblown ash was postdepositionally remobilized to source these deposits is unknown, but we speculate that no deposits would be likely without at least several millimeters of ash fall in this region.

Ash deposits in northern California and southern Oregon are easily explainable under the influence of a rapidly expanding umbrella cloud, even if prevailing winds were unfavorable to westerly transport (which is poorly known at 2.1 Ma and 640 ka). Without an umbrella cloud, westward transport may still occur within high-level easterly winds (A. Sarna, written communication, 2014) (e.g., Figure 9b), but less frequently, at least under present-day wind patterns (Figure 4). This again points to the important role of outward (umbrella) expansion in transport of ash from large-scale eruptions. Yellowstone’s Lava Creek B ash bed has also been found in cores from Tulelake on the California-Oregon border [Rieck et al., 1992] (Figure 1), and Huckleberry Ridge deposits are located in Deep-Sea Drill Site 36 in the eastern Pacific (Figure 1). The offshore deposits are not likely to have been transported fluvially from onshore [Sarna-Wojcicki et al., 1987]. These occurrences are readily explained by an umbrella cloud extending at least 1500 km westward of Yellowstone, although transport to DSDP site 36 may require both an umbrella cloud and favorable winds (e.g., Figures 7a, 8a, and 8c).

6. Conclusions

Geological activity at Yellowstone provides no signs that a supereruption will occur in the near future. Indeed, current seismicity, crustal deformation and thermal activity are consistent with the range and

Table A1. Model Parameters Used to Simulate Growth of the 15 June 1991 Umbrella Cloud at Pinatubo

Parameter	Value(s)
Eruption start time (UTC)	15 Jun 1991, 0440UTC (1340 local time)
Height of top of umbrella cloud	25 km
Duration	9 h
Erupted volume	6 km ³ DRE (1.5×10 ¹³ kg)
Model domain	89.558–132.454° longitude 1.227–28.846° latitude
Model resolution	0.2° horizontally, 2 km vertically
Grain sizes	One grain size 0.01 mm diameter 1000 kg m ⁻³ density
Diffusion constant	0 m ² s ⁻¹
k_e	0.1
N	0.02 s ⁻¹
C	0.5×10 ⁴ m ³ kg ^{-3/4} s ^{-7/8}
λ	0.2

magnitude of signals observed historically over the past century [Lowenstern *et al.*, 2006]. Over the past two million years, trends in the volume of eruptions and the magnitude of crustal melting may signal a decline of major volcanism from the Yellowstone region [Christiansen *et al.*, 2007; Watts *et al.*, 2012]. These factors, plus the 3-in-2.1-million annual frequency of past events, suggest a confidence of at least 99.9% that 21st-century society will not experience

a Yellowstone supereruption. But over the span of geologic time, supereruptions have recurred somewhere on Earth every 100,000 years on average [Mason *et al.*, 2004; Sparks *et al.*, 2005]. As such, it is important to characterize the potential effects of such events. We hope this work stimulates further examination of ash transport during very large eruptions.

Appendix A: Simulating the Growth of the Pinatubo Umbrella Cloud

We validate the umbrella cloud formulation by simulating the growth of the 15 June 1991 umbrella cloud at Pinatubo. This is the only large umbrella cloud observed with modern techniques and its growth has been examined in numerous studies. The model setup and atmospheric parameters are indicated in Table A1. For meteorological conditions we use the RE1 wind field. Typhoon Yunya prevented the launching of radiosondes during the eruption [Fero *et al.*, 2009] and limited the accuracy of modeled wind fields. Thus we, like others [Costa *et al.*, 2013; Fero *et al.*, 2009], had to rotate wind directions 30 degrees counterclockwise to match the observed direction of cloud movement.

Our umbrella-cloud formulation requires a single eruptive pulse of constant rate and umbrella-cloud height. We use a starting time at 1340 Pinatubo Daylight Time (0440 UTC) on 15 June 1991; a duration of 9 h; and an umbrella-cloud height of 25 km, which corresponds to the cloud top observed in satellite images [Holasek *et al.*, 1996; Koyaguchi and Tokuno, 1993], but is lower than the 35–40 km of the overshooting top [Holasek *et al.*, 1996]. The erupted volume has been estimated 4.8–6.0 km³ DRE from deposits [Wiesner *et al.*, 2004, 2005]. We use an erupted volume of 6 km³ DRE, and assume a magma density of 2500 kg m⁻³.

Figure A1 (a) shows hourly outlines of the observed cloud perimeter starting at 1440 PDT, digitized from Fig. 5b of Holasek *et al.* [1996]. Figure A1 (b) shows outlines of the cloud at the same times, based on the Ash3d simulation. The result illustrates reasonably good agreement. Figure A2 shows cloud diameter versus time obtained from the observations of Holasek *et al.* [1996, Fig. 5b], from the Ash3d simulation, and from same theoretical method used in Fig. 5a, assuming an erupted volume of 6 (dashed line) or 10 (solid line) km³ DRE. For the Holasek *et al.* and Ash3d results, cloud diameter d was determined by measuring the cloud area A and using the formula $d = 2\sqrt{A/\pi}$. The Ash3d cloud diameters agree surprisingly well with those of Holasek *et al.*, especially given that the simulation assumed a constant eruption rate with time.

References

- Bacon, C. R. (1983), Eruptive history of Mount Mazama and Crater Lake Caldera, Cascade Range, U.S.A., *J. Volcanol. Geotherm. Res.*, 18, 57–115.
- Baines, P. G., and R. S. J. Sparks (2005), Dynamics of giant volcanic ash clouds from supervolcanic eruptions, *Geophys. Res. Lett.*, 32, L24808, doi:10.1029/2005GL024597.
- Bonadonna, C., J. C. Phillips, and B. F. Houghton (2005), Modeling tephra sedimentation from a Ruapehu weak plume eruption, *J. Geophys. Res.*, 110, B08209, doi:10.1029/2004JB003515.
- Carey, S., and R. S. J. Sparks (1986), Quantitative models of the fallout and dispersal of tephra from volcanic eruption columns, *Bull. Volcanol.*, 48, 109–125.
- Christiansen, R. L. (2001), The Quaternary and Pliocene Yellowstone Plateau Volcanic Field of Wyoming, Idaho, and Montana, *U.S. Geol. Surv. Prof. Pap.* 729-G, U.S. Gov. Print. Off., Washington, D. C.
- Christiansen, R. L., and H. R. Blank Jr. (1972), Volcanic stratigraphy of the Quaternary rhyolite plateau in Yellowstone National Park, Wyoming, *U.S. Geol. Surv. Prof. Pap.*, 729-B, 18 pp.

Acknowledgments

We thank reviewers Andrei Sarna-Wojcicki, Robert L. Christiansen, and Manuel Nathenson for comments that improved the paper. We would also like to express our gratitude to an anonymous reviewer who recommended incorporation of an expanding umbrella cloud into Ash3d, and pointed us to the approach of Costa *et al.* [2013]. Second author AVE acknowledges NSF Postdoctoral Fellowship EAR1250029 for funding at the time of her contribution to this work. The data and model results used in this paper have been posted as supporting information. The supporting information includes input files and ASCII or kmz output files that can be opened in ArcMap® or Google Earth® software (use of trade names does not imply endorsement of these products by the U.S. Government).

- Christiansen, R. L., J. B. Lowenstern, R. B. Smith, H. Heasler, L. A. Morgan, M. Nathenson, L. G. Mastin, L. J. P. Muffler, and J. E. Robinson (2007), Preliminary assessment of volcanic and hydrothermal hazards in Yellowstone National Park and vicinity, *U.S. Geol. Surv. Open File Rep. 2007-1071*, p. 94, U.S. Gov. Print. Off., Washington, D. C.
- Cornell, W., S. Carey, and H. Sigurdsson (1983), Computer simulation of transport and deposition of the campanian Y-5 ash, *J. Volcanol. Geotherm. Res.*, 17(1-4), 89–109.
- Costa, A., A. Folch, and G. Macedonio (2013), Density-driven transport in the umbrella region of volcanic clouds: Implications for tephra dispersion models, *Geophys. Res. Lett.*, 40, 4823–4827, doi:10.1002/grl.50942.
- Cramp, A., C. Vitaliano, and M. Collins (1989), Identification and dispersion of the campanian ash layer (Y-5) in the sediments of the Eastern Mediterranean, *Geo Mar. Lett.*, 9(1), 19–25, doi:10.1007/BF02262814.
- Di Lorenzo, E., K. M. Cobb, J. C. Furtado, N. Schneider, B. T. Anderson, A. Bracco, M. A. Alexander, and D. J. Vimont (2010), Central Pacific El Niño and decadal climate change in the North Pacific Ocean, *Nat. Geosci.*, 3(11), 762–765. [Available at <http://www.nature.com/ngEO/journal/v3/n11/abs/ngEO984.html#supplementary-information>.]
- Dobson, P. F., L. Sienkiewicz, and R. A. Armin (1991), Origin of thick ash-rich sediments in the northern Gulf of Mexico, *Geol. Soc. Am. Abstr. Programs*, 23(5), A258.
- Durant, A. J., W. I. Rose, A. M. Sarna-Wojcicki, S. Carey, and A. C. Volentik (2009), Hydrometeor-enhanced tephra sedimentation: Constraints from the 18 May 1980 eruption of Mount St. Helens (USA), *J. Geophys. Res.*, 114, B03204, doi:10.1029/2008JB005756.
- Fero, J., S. N. Carey, and J. T. Merrill (2009), Simulating the dispersal of tephra from the 1991 Pinatubo eruption: Implications for the formation of widespread ash layers, *J. Volcanol. Geotherm. Res.*, 186(1–2), 120–131, doi:10.1016/j.jvolgeores.2009.03.011.
- Fierstein, J., and M. Nathenson (1992), Another look at the calculation of fallout tephra volumes, *Bull. Volcanol.*, 54, 156–167.
- Folch, A., A. Costa, and G. Macedonio (2009), FALL3D: A computational model for transport and deposition of volcanic ash, *Comput. Geosci.*, 35(6), 1334–1342, doi:10.1016/j.cageo.2008.08.008.
- Gudmundsson, M. T., et al. (2012), Ash generation and distribution from the April–May 2010 eruption of Eyjafjallajökull, Iceland, *Sci. Rep.*, 2(572), doi:10.1038/srep00572.
- Guffanti, M., G. Mayberry, T. Casadevall, and R. Wunderman (2009), Volcanic hazards to airports, *Nat. Hazards*, 51(2), 287–302, doi:10.1007/s11069-008-9254-2.
- Hildreth, W. (1983), The compositionally zoned eruption of 1912 in the Valley of Ten Thousand Smokes, Katmai National Park, Alaska, *J. Volcanol. Geotherm. Res.*, 18, 1–56.
- Hildreth, W. and R. E. Drake (1992), Volcán Quizapu, Chilean Andes, *Bull. Volcanol.*, 54, 93–125.
- Holasek, R. E., S. Self and A. W. Woods (1996), Satellite observations and interpretation of the 1991 Mount Pinatubo eruption plumes, *J. Geophys. Res.*, 101(B12), 27,635–27,656, doi:10.1029/96JB01179.
- Horwell, C. J., and P. J. Baxter (2006), The respiratory health hazards of volcanic ash: A review for volcanic risk mitigation, *Bull. Volcanol.*, 69(1), 1–24, doi:10.1007/s00445-006-0052-y.
- Izett, G. A., and R. E. Wilcox (1982), Map showing localities and inferred distributions of the Huckleberry Ridge, Mesa Falls and Lava Creek ash beds (Pearlette family ash beds) of Pliocene and Pleistocene age in the western United States and southern Canada, *U.S. Geol. Surv. Misc. Invest. Map I-1325*, scale 1:4,000,000, U.S. Geological Survey, Washington, D. C.
- Kalnay, E., et al. (1996), The NCEP/NCAR 40-Year Reanalysis Project, *Bull. Am. Meteorol. Soc.*, 77(3), 437–471, doi:10.1175/1520-0477(1996)077<0437:TNYRP>2.0.CO;2.
- Koyaguchi, T., and M. Ohno (2001), Reconstruction of eruption column dynamics on the basis of grain size of tephra fall deposits: 2. Application to the Pinatubo 1991 eruption, *J. Geophys. Res.*, 106(B4), 6513–6533, doi:10.1029/2000JB900427.
- Koyaguchi, T., and M. Tokuno (1993), Origin of the giant eruption cloud of Pinatubo, June 15, 1991, *J. Volcanol. Geotherm. Res.*, 55, 85–96.
- Lowenstern, J. B., R. B. Smith, and D. P. Hill (2006), Monitoring super-volcanoes: Geophysical and geochemical signals at Yellowstone and other large caldera systems, *Philos. Trans. R. Soc. A*, 364(1845), 2055–2072, doi:10.1098/rsta.2006.1813.
- Mantua, N. J., and S. R. Hare (2002), The Pacific decadal oscillation, *J. Oceanogr.*, 58(1), 35–44, doi:10.1023/A:1015820616384.
- Mason, B. G., D. M. Pyle, and C. Oppenheimer (2004), The size and frequency of the largest eruptions on Earth, *Bulletin of Volcanology*, vol. 66, pp. 735–748, doi:10.1007/s00445-004-0355-9.
- Mastin, L. G., et al. (2009), A multidisciplinary effort to assign realistic source parameters to models of volcanic ash-cloud transport and dispersion during eruptions, *J. Volcanol. Geotherm. Res.*, 186, 10–21.
- Mastin, L. G., A. Van Eaton, A. Durant, H. Schwaiger, and R. Denlinger (2013a), Towards an operational implementation of particle aggregation in ash dispersion models, Abstract V21D-04 presented at 2013 Fall Meeting, AGU, San Francisco, Calif.
- Mastin, L. G., H. Schwaiger, D. J. Schneider, K. L. Wallace, J. Schaefer, and R. P. Denlinger (2013b), Injection, transport, and deposition of tephra during event 5 at Redoubt Volcano, 23 March, 2009, *J. Volcanol. Geotherm. Res.*, 259, 201–213, doi:10.1016/j.jvolgeores.2012.04.025.
- Morton, B. R., G. I. Taylor, and J. S. Turner (1956), Turbulent gravitational convection from maintained and instantaneous sources, *Proc. R. Soc. London, Ser. A*, 234, 1–23.
- Newhall, C. G., and R. Punongbayan (Eds.) (1996), *Fire and Mud: Eruptions and Lahars of Mount Pinatubo, Philippines*, 1126 pp., Univ. of Wash. Press, Seattle.
- Oppenheimer, C. (2003), Climatic, environmental and human consequences of the largest known historic eruption: Tambora volcano (Indonesia) 1815, *Prog. Phys. Geogr.*, 27(2), 230–259, doi:10.1191/0309133303pp379ra.
- Pallister, J. S., R. P. Hoblitt, D. R. Crandell, and D. R. Mullineaux (1992), Mount St. Helens a decade after the 1980 eruptions: Magmatic models, chemical cycles, and a revised hazards assessment, *Bull. Volcanol.*, 54, 126–146.
- Pyle, D. M. (1989), The thickness, volume and grain size of tephra fall deposits, *Bull. Volcanol.*, 51, 1–15.
- Rieck, H. J., A. M. Sarna-Wojcicki, C. E. Meyer, and D. P. Adam (1992), Magnetostratigraphy and tephrochronology of an upper Pliocene to Holocene record in lake sediments at Tulelake, northern California, *Geol. Soc. Am. Bull.*, 104(4), 409–428, doi:10.1130/0016-7606(1992)104<0409:matoau>2.3.co;2.
- Rose, W. I., and C. A. Chesner (1987), Dispersal of ash in the great Toba eruption, 75 ka, *Geology*, 15(10), 913–917, doi:10.1130/0091-7613(1987)15<913:doaitg>2.0.co;2.
- Sarna-Wojcicki, A. M. (2000), Tephrochronology, in *Quaternary Geochronology: Methods and Applications*, AGU Ref. Shelf 4, edited by J. S. Noller, J. M. Sowers, and W. R. Lettis, pp. 357–377, AGU, Washington, D. C.
- Sarna-Wojcicki, A. M., S. D. Morrison, C. E. Meyer, and J. W. Hillhouse (1987), Correlation of upper Cenozoic tephra layers between sediments of the western United States and eastern Pacific Ocean and comparison with biostratigraphic and magnetostratigraphic age data, *Geol. Soc. Am. Bull.*, 98(2), 207–223, doi:10.1130/0016-7606(1987)98<207:couct1>2.0.co;2.

- Schwaiger, H., R. Denlinger, and L. G. Mastin (2012), Ash3d: A finite-volume, conservative numerical model for ash transport and tephra deposition, *J. Geophys. Res.*, *117*, B04204, doi:10.1029/2011JB008968.
- Self, S. (2006), The effects and consequences of very large explosive volcanic eruptions, *Philos. Trans. R. Soc. A*, *364*, 2073–2097, doi:10.1098/rsta.2006.1814.
- Self, S., M. R. Rampino, M. S. Newton, and J. Wolff (1984), Volcanological study of the great Tambora eruption of 1815, *Geology*, *12*(11), 659–663.
- Simkin, T. L., and R. S. Fiske (1983), *Krakatau 1883: The Volcanic Eruption and Its Effects*, 464 pp., Smithsonian Inst., Washington, D. C.
- Sorem, R. K. (1982), Volcanic ash clusters: Tephra rafts and scavengers, *J. Volcanol. Geotherm. Res.*, *13*, 63–71.
- Sparks, R. S. J. (1986), The dimensions and dynamics of volcanic eruption columns, *Bull. Volcanol.*, *48*(1), 3–15, doi:10.1007/BF01073509.
- Sparks, R. S. J., J. G. Moore and C. J. Rice (1986), The initial giant umbrella cloud of the May 18th, 1980, explosive eruption of Mount St. Helens, *J. Volcanol. Geotherm. Res.*, *28*(3–4), 257–274.
- Sparks, R. S. J., M. I. Bursik, S. N. Carey, J. S. Gilbert, L. S. Glaze, H. Sigurdsson and A. W. Woods (1997), *Volcanic Plumes*, 574 pp., John Wiley, Chichester, U. K.
- Sparks, R. S. J., S. Self, J. Gratten, C. Oppenheimer, D. M. Pyle, and H. Rymer (2005), *Supereruptions: Global Effects and Future Threats, Report of a Geological Society Working Group*, 25 pp., Geological Society of London, London, U. K.
- Suzuki, T. (1983), A Theoretical model for dispersion of tephra, in *Arc Volcanism: Physics and Tectonics*, edited by D. Shimozuru and I. Yokoyama, pp. 95–113, Terra Sci. Publ. Co., Tokyo.
- Suzuki, Y. J., and T. Koyaguchi (2009), A three-dimensional numerical simulation of spreading umbrella clouds, *J. Geophys. Res.*, *114*, B03209, doi:10.1029/2007JB005369.
- Van Eaton, A. R., J. D. Muirhead, C. J. N. Wilson and C. Cimarelli (2012), Growth of volcanic ash aggregates in the presence of liquid water and ice: An experimental approach, *Bull. Volcanol.*, *74*(9), 1963–1984, doi:10.1007/s00445-012-0634-9.
- Wallace, K. L., J. R. Schaefer, and M. L. Coombs (2013), Character, mass, distribution, and origin of tephra-fall deposits from the 2009 eruption of Redoubt Volcano, Alaska—Highlighting the significance of particle aggregation, *J. Volcanol. Geotherm. Res.*, *259*, 145–169, doi:10.1016/j.jvolgeores.2012.09.015.
- Watts, K. E., I. Bindeman, and A. K. Schmitt (2012), Crystal-scale anatomy of a dying supervolcano: An isotope and geochronology study of individual phenocrysts from voluminous rhyolites of the Yellowstone Caldera, *Contrib. Mineral. Petrol.*, *164*, 45–67.
- Wiesner, M., A. Wetzel, S. Catane, E. Listanco, and H. Mirabueno (2004), Grain size, areal thickness distribution and controls on sedimentation of the 1991 Mount Pinatubo tephra layer in the South China Sea, *Bull. Volcanol.*, *66*(3), 226–242, doi:10.1007/s00445-003-0306-x.
- Wiesner, M., A. Wetzel, S. Catane, E. Listanco, and H. Mirabueno (2005), Grain size, areal thickness distribution and controls on sedimentation of the 1991 Mount Pinatubo tephra layer in the South China Sea, *Bull. Volcanol.*, *67*(5), 490–495, doi:10.1007/s00445-005-0421-y.
- Wilcox, R. E., and C. W. Naeser (1992), The Pearlette family ash beds in the Great Plains: Finding their identities and their roots in the Yellowstone country, *Quat. Int.*, *13–14*, 9–13, doi:10.1016/1040-6182(92)90003-K.
- Wilson, C. J. N. (2001), The 26.5ka Oruanui eruption, New Zealand: An introduction and overview, *J. Volcanol. Geotherm. Res.*, *112*(1–4), 133–174, doi:10.1016/S0377-0273(01)00239-6.
- Wilson, C. J. N. (2008), Supereruptions and supervolcanoes: Processes and products, *Elements*, *4*, 29–34.
- Wilson, C. J. N., and W. Hildreth (1997), The Bishop Tuff: New insights from eruptive stratigraphy, *J. Geol.*, *105*, 407–439.
- Wilson, L., and T. C. Huang (1979), The influence of shape on the atmospheric settling velocity of volcanic ash particles, *Earth Planet. Sci. Lett.*, *44*, 311–324.
- Wilson, T. M., C. Stewart, V. Sword-Daniels, G. S. Leonard, D. M. Johnston, J. W. Cole, J. Wardman, G. Wilson and S. T. Barnard (2012), Volcanic ash impacts on critical infrastructure, *Phys. Chem. Earth*, *45–46*, 5–23, doi:10.1016/j.pce.2011.06.006.